Improve Land Surface Emissivity Parameter for Land Surface Models Using Global Remote Sensing Observations

Menglin Jin[1]
Shunlin Liang[2]
1. Department of Atmospheric and Oceanic Science, University of Maryland, College Park, mjin@atmos.umd.edu, Office: 301-405-8833
2. Department of Geography, University of Maryland, College Park

June, 2005
Accepted by J. of Climate

Abstract

Because land surface emissivity (ε) had not been reliably measured, global climate model's (GCM) land surface schemes conventionally simply set this parameter as constant, for example 1 as in the National Oceanic and Atmospheric Administration (NOAA) National Centers for Environmental Prediction (NCEP) model and 0.96 for bare soil as in the National Center for Atmospheric Research (NCAR) Community Land Model (CLM2). This is so-called "constant-emissivity assumption". Accurate broadband emissivity data are needed as a model input to better simulate land surface climate. We demonstrate in this paper that the assumption of the constant emissivity induces errors in modeling the surface energy budget, especially over large arid and semi-arid areas where ε is far smaller than unity. One feasible solution to this problem is to apply the satellite-based broadband emissivity into land surface models.

The Moderate Resolution Imaging Spectroradiometer (MODIS) instrument has routinely measured spectral emissivities (ε_λ) in six thermal infrared bands. The empirical regression equations have been developed in this study to convert these spectral emissivities to broadband emissivity (ε) required by land surface models. The observed emissivity data show strong seasonality and land-cover dependence. Specifically, emissivity depends on surface cover type, soil moisture content, soil organic composition, vegetation density and structure. For example, broadband ε is usually around 0.96-0.98

for densely vegetated areas (leaf area index LAI>2), but it can be lower than 0.90 for bare soils (e.g., desert). To examine the impact of variable surface broadband emissivity, we conducted sensitivity studies using offline CLM2 and coupled NCAR Community Atmosphere Model CAM2/CLM2. These sensitivity studies illustrate that large impacts of surface ε occur over deserts, with change up to 1-2°C in ground temperature, surface skin temperature, and 2m surface air temperature, as well as evident changes in sensible and latent heat fluxes.

1. Introduction

Emissivity (ε) is the ratio of energy emitted from a natural material to that from an ideal blackbody at the same temperature. Accurate surface ε is desired in land surface models for better simulations of surface energy budgets from which skin temperature in the model is calculated (Jin et al. 1997). Lacking global ε observations, the first comprehensive land surface models coupled to general circulation models (GCMs) simply assumed ε as 1 (Dickinson et al. 1986; Sellers et al. 1987). Later many land surface models adopted this assumption by setting ε as 1 or constants close to 1. Although the constant-ε [1]assumption provides first-order approximation, it induces errors in simulating surface-upward longwave radiation and, consequently, radiative energy redistribution. Although constant-ε assumption may be valid for most vegetated areas where ε is close to unity, it is not true for arid and semi-arid areas. For example, ε = 0.7-0.8 were observed over the Saharan deserts at 9μm due to large quartz levels there (Rowntree 1991; Prabhakara and Dalu 1976), and thus assuming ε=1 may result in an error of about 15Wm^{-2} in the net longwave radiation annually given the fact that the desert surface emissivity is 0.90 in many areas from MODIS observation and the annual

[1] Here the "constant-ε" assumption means two-fold problem. First, ε is assumed to be constant when it actually varies in space and time. Second, the ε is assumed to be near one, which is incorrect for certain surfaces.

net longwave radiation is about 160Wm^{-2} (See Figure 1 and Eq. (8)). The instantaneous error may be higher when the surface net radiation is above the annual mean.

In Community Land Model version 2.0, the land surface model of the National Center for Atmospheric Research (NCAR CLM2), there are three surface emissivities: bare soil emissivity, canopy emissivity (ε_c), and snow emissivity. Except that ε_c is calculated very simply as a function of leaf area index (LAI), the other emissivity values are prescribed as 0.96 for soil and 0.97 for snow, respectively. Therefore, emissivity treatment is still a problem in CLM2 when soil emissivity is set as constant since this variable can shift more than 10% around the globe from MODIS observations we present below.

The goal of this work is to examine whether the constant-ε assumption currently used in land surface models is realistic, and to study the impact of ε on land surface modeling. To achieve that, we employed two methods. First, the emissivity products from MODIS (Moderate-Resolution Imaging Spectroradiometer) were analyzed to demonstrate the global distribution, seasonal variation, and ε-LAI relationship. Second, the NCAR offline CLM2 and NCAR Community Atmosphere Model coupled with CLM2 (CAM/CLM2) were used to conduct a series of sensitivity studies.

Remotely sensing surface ε is very challenging because of the high heterogeneity of land surfaces and the difficulties in removing atmospheric effects (Wan and Li 1997; Liang 2001, 2003). Furthermore, there is a mismatch between what remote sensing provides and what land surface models need: remote sensing measures spectral emissivity (ε_λ)

through channels at certain wavelength (λ) but land surface models need "broadband" emissivity for calculating upward longwave radiation using the Stefan-Boltzmann law. Due to atmospheric absorption, only the spectral radiance within the infrared water vapor window region (i.e., 8-14μm) is measured by thermal infrared remote sensing. It is these measurements that need to be converted into broadband emissivity. In this study, a regression equation based on radiative transfer model is derived to convert MODIS spectral emissivities into broadband emissivity. More details are available in Section 2.3.

In the remaining part of this paper, section 2 describes the properties of emissivity and its role in land surface equations. Section 3 introduces the observations and the models used in this work. Sections 4 and 5 present results, discussions, and conclusions.

2. Background

2.1 Properties of emissivity

Conceptually, all materials are formed by molecules with atoms bonded together inside through molecular bonds. Atoms vibrate at the end of a bond when agitated by light of particular wavelength hitting the molecule. In turn, the molecule re-emits the same wavelength of light. This is the "absorption and emission" process. Only light in the infrared spectrum causes molecular vibration. Since every unique molecule has its own characteristic frequency of vibration, a natural surface emits the infrared light depends on surface composition, namely the emissivity spectrum , is distinct depending on

surface composition. Simply put, if the surface is of mixed types, it has different emissivities.

Emissivity is defined as:

$$\varepsilon_\lambda = E_\lambda / B_\lambda(T), \quad (1)$$

where E_λ is emitted radiance at wavelength λ and $B_\lambda(T)$ is blackbody emission at wavelength λ and temperature T. $B_\lambda(T)$ can be calculated from the Planck function.

Kirchoff's Law states that the emissivity of an opaque body at thermodynamic equilibrium is equal to absorptivity, and therefore based on the conservation of energy, the reflectivity R_λ and emissivity is

$$R_\lambda = 1 - \varepsilon_{\lambda,} \quad (2)$$

It is difficult to determine the emissivity of an object for at least three reasons: emissivity is a surface property, and the surface of an object may change with time; the land surface is composed of various objects with different emissivities; and emissivity retrieval from remote sensing depends on the surface temperature, but accurate surface temperature is difficult to measure.

Emissivity of bare soil

The emissivity of natural land surface is determined by soil structure, soil composition, organic matter, moisture content and vegetation cover characteristics (Van De Griend and

Owe 1993), but does not depend on soil temperature profile or surface temperature. For bare soil, the key parameters affecting emissivity are the surface finish, the chemical composition, the soil's thermal and mechanical history, and the wavelength at which the emissivity is measured (Van De Griend and Owe 1993). Physically, emissivity is independent of bare soil temperature, but since thermal infrared radiance measured by satellite radiometer includes signals of both temperature and emissivity, emissivity has to be separated from temperature (Snyder et al. 1998).

Emissivity is determined partially by grain sizes of soil and organic content. Nerry et al. (1990) reported that the smaller the diameter of soil grain, the higher the emissivity over 10-14 μm from a sample of SiC sands (see their Figure 7). The decrease of spectral contrast with decreasing grain-size diameter is a well-known effect (Logan et al. 1974) in a region where surface scattering dominates.

Land surface models require emissivity integrated over the longwave water vapor window region 8-14μm. Therefore, for the purpose of understanding the impact of emissivity on model predictions, our study focuses only on this spectral region. Table 1 presents reference values of emissivity for some materials. It shows that emissivity varies significantly with chemical materials; therefore, the soil emissivity of a given sample is sensitive to its chemical compositions. Furthermore, environmental effects over the history of these chemical components may cause changes in properties (e.g, surface roughnessor surface contamination) that affect emissivity (Francois et al. 1997).

Emissivity of Canopy

Emissivity of canopy, ε_c, is even more complex than the underlying soil emissivity. Single leaf emissivity differs from that of integrated effective canopy emissivity (Fuchs and Tanner 1996, Van De Griend and Owe 1993, Francois et al. 1997), because ε_c is determined by the overall structure of the vegetation instead of the flat surface of leaves (the "cavity effect"). Cavity effects make ε_c larger than the single leaf's ε due to multiple internal reflections resulting from canopy geometry structure. For example, ε is from 0.95 to 0.98 for single leaves but is expected to increase for dense canopy (Fuchs and Tanner 1966). Idso et al. (1969) reported a leaf emissivity as low as 0.938. It was found that the cavity effect becomes significant when the leaves' proportion exceeds the soil proportion (namely, about leaf area index LAI>2). In addition, although different leaves show similar spectral reflectances in both visible and near-infrared wavelengths, distinct features of emissivity are noticed in the thermal-infrared region.

The plant species, vegetation density and growth state all affect ε_c. Using a radiative transfer model, Francois et al. (1997) reported that as canopy LAI, the variable representing the greenness and density of vegetation from remote sensing, increases, the ε_c increases --to a limit. Their model finds that LAI profile, namely vegetation vertical structure, has little effect on ε. The view angle modifies ε_c only for off-zenith angles greater than 50º.

A good review of ε and vegetation index was provided by Van De Griend and Owe (1993). Measured over a savanna environment, they found that thermal emissivity was highly positively correlated with Normalized Difference Vegetation Index (NDVI) with a correlation coefficient as high as 0.94. Their field experiments measured ε = 0.914 for bare soil of loamy sand (NDVI=0.157), 0.949 for partly covered open grass (NDVI = 0.278), 0.958 for long grass (NDVI = 0.276), 0.952 for partly covered shrub with NDVI as 0.367, and 0.986 for completely covered shrub when NDVI = 0.727. Following these measurements, they developed one logarithmic equation to describe the empirical relations between ε and NDVI. Note that their results were based on field experiment and only for savanna; the application of their values in land surface model needs further verification for other vegetation types.

There are other factors affecting ε_c. Dynamic states of vegetation such as growing crops and idle crops (bare soil) have distinct ε (Snyder et al. 1998). In addition, water stress, for example, could also have some effect on the canopy emissivity (Francois et. al. 1997).

2.2 Emissivity in land surface model

The exchanges of momentum, heat, and moisture at the land surface in an atmosphere-vegetation-soil system are the key physical processes that determine the land surface thermodynamics and dynamics. The unique role of ε can be demonstrated in the energy balance equation that governs the heat and water exchanges:

$$R_n = SH+LE+G, \quad (3)$$

$$R_n = S_{\downarrow}-S_{\uparrow}+LW_{\downarrow}-LW_{\uparrow}, \quad (4)$$

$$LW_{\uparrow}=\varepsilon\sigma T_s^4, \quad (5)$$

where SH is sensible heat flux, LE is latent heat flux, and G is the ground heat flux. These three processes compete for surface net radiation R_n, which is the downward minus upward shortwave and longwave radiation. In Eq. (4), $S_{\downarrow}$ is downward solar radiation, $S_{\uparrow}$ is reflected solar radiation, $LW_{\downarrow}$ is downward longwave radiation, and LW↑ is upward longwave radiation from the surface. Emissivity and surface skin temperature (T_s) determine the upward longwave radiation, or surface emission, following the Stefan-Boltzmann Law.

We first theoretically analyze the possible ε effect. To keep the discussion simple, here we only analyze the case when the ε=1, for it gives maximum errors. If ε is set to 1, net longwave radiation is:

$$LW_n^{\varepsilon=1} = LW\downarrow- \sigma T_s^4, \quad (6)$$

while, in fact, this term should be:

$$LW_n^{\varepsilon\neq1} = LW\downarrow-\varepsilon \sigma T_s^4 -(1-\varepsilon)LW\downarrow \quad (7)$$

Therefore, the error induced by the unit emissivity assumption is:

$$\Delta = LW_n^{\varepsilon \neq 1} - LW_n^{\varepsilon = 1}$$

$$= \underline{(\sigma T_s^4 - LW\downarrow)}\ \underline{(1-\varepsilon)}. \qquad (8)$$

$$\text{A} \qquad \text{B}$$

Δ is the error on net longwave radiation if accurate ε is not taken into account in land surface models. Eq. (8) implies two situations when large errors may occur due to inaccurate ε: where there are large differences between upward and downward longwave radiation (term A), and where the surface ε greatly departs from unit (term B).

We used the National Oceanic and Atmospheric Administration (NOAA) National Centers for Environmental Prediction (NCEP) reanalysis to examine when and where the first situations may occur. Figure 1 shows the magnitude of term A of Eq. (8) over the globe. These analyses were based on the NCEP reanalysis for July, November and the annual mean for the year 2001, respectively. Large net longwave radiation centers are shown over desert areas including the Sahara, Australia, southwest North America, and the central desert areas of Eurasia. These deserts are associated by hot, downwelling branches of the Hadley circulation. With the displacement of general circulation in different seasons, the strength and locations of the net longwave radiation centers vary moderately from season to season. For example, the maximum for term A is in the Sahara in July but moves to Eurasia in November, with values of $166 Wm^{-2}$ and $155 Wm^{-2}$, respectively. Meanwhile, as bare soil with little moisture and vegetation, these areas have

small ε values that are far from 1; therefore, large Δ are expected to occur over these areas. The Sahara, for instance, may have annual mean Δ around 15Wm^2, given term A about 160 Wm^2 and emissivity of 0.90 (see section 4). This instaneous error maybe higher term A. This Δ will propagate an error in skin temperature and heat fluxes, as we prove later. For non-desert regions, where emissivity is higher and term A is smaller, the constant emissivity assumption may be tolerable. We will use model sensitivity studies to examine this posssible tolerance in Section 3.

2.3 Broadband emissivity conversion

Remote sensing retrieves emissivity from individual spectral bands (i.e., ε_λ) while GCM's land surface model needs "broadband" emissivity (i.e., ε). Therefore, a conversion from narrowband into broadband is necessary. Outside of the water vapor window, $LW_\downarrow$ originates from the levels close to the ground and thus differs little from the surface emission. Consequently, only surface radiation at the window region is critical for the surface radiation budget (Rowntree 1991, Dickinson personal communications). In other words, only window region spectral emissivity needs to be taken into account during spectral-broadband emissivity conversion. Note that even in the water vapor window, the presence of clouds will increase the downwelling longwave above its clear sky value, and thus reduce the delta described by equation (8). Nevertheless, for desert and semi-desert regions, clouds effect is ignorable.

Figure 2 shows the variation of emissivity as a function of wavelength for soil. Evidently, for different samples of soil, ε_λ is different because of the differing chemical composition of the soils. The ε_λ varies from 0.91 at 9.1μm to 0.98 at 14.5μm. The spectral emissivity value in Figure 2 beyond 14.5μm is not reliable due to the strong atmospheric absorption. The large irregular variations with wavelength make it difficult to derive a "broadband" ε. In this work, we conducted extensive simulations incorporating thousands of surface emissivity spectra, and then derived the regression equations as the function of the Moderate Resolution Imaging Spectroradiometer (MODIS) spectral emissivity values. Broadband ε should be seen as a first-order approximation for capturing the integrated features of ε from MODIS spectral bands.

The procedure for developing conversion formulae of spectral emissivities to broadband emissivity consists of the following steps. First, thousands of measured emissivity spectra from different sources (e.g., Advanced Spaceborne Thermal Emission and Reflection Radiometer (ASTER) spectral library, Salisbury database, US Geological Survey spectral library) have been collected. Second, broadband "effective" emissivity is calculated using the Planck equation and spectral emissivity spectra. Third, integrating these surface spectral emissivity spectra with the sensor spectral response functions leads to the simulated MODIS spectral emissivities. Finally, a linear relationship is established between the broadband emissivity (ε) and MODIS spectral emissivities (ε_i) through regression analysis:

$$\varepsilon_{8\text{-}14} = 0.0281+0.2863\varepsilon_{29}+0.4407\varepsilon_{31}+0.2399\varepsilon_{32} \quad (10)$$

Although MODIS has four bands in 8-12 μm (bands 29-32[2]), not all of them are incorporated in the formula above because of their correlation and large uncertainties in estimating the spectral emissivity at band 30.

MODIS has two different algorithms for estimating spectral emissivities (Wan and Li 1997). One of them is based on land cover information that may determine the spectral emissivity in bands 31 and 32 far more accurately than other bands. If only emissivities of bands 31 and 32 are used, the formula is

$$\varepsilon_{8-14} = 0.4587\varepsilon_{31} + 0.5414\varepsilon_{32} \quad (11)$$

Nevertheless, the broadband emissivity estimated only from emissivities in MODIS bands 31 and 32 (Eq. 11) may not be too accurate, because of lacking information in the 8-8.7μm spectral range, where emissivities of soils and minerals may vary significantly. As a conclusion, we recommend Equations (10) as a more standard conversion approach.

In general, uncertainty of spectral band emissivity is 0.001-0.005 for each band (Wan and Li 1997). Such uncertainty will likely propagate into the final broadband emissivity value. In addition, uncertainty exists using the regression equation to convert spectral

[2] Band 29 is 8.400-8.700 μm; band 31 is 10.780-11.280 μm; and band 32 is 11.770-12.270 μm.

band to broadband. Figure 4 is the comparison of 3 band converted ε (MODIS band 29, 31 32) and radiative transfer model simulated broadband emissivity. Our assessment show that such uncertainty is about +/-0.005.

3. Data and Model

Monthly mean MODIS observations are used to examine the geographical distributions of ε. The emissivity values in the Version 4 MODIS Land-Surface Temperature/Emissivity product (MOD11B1) at 5km Sinusoidal grids were obtained from the MODIS science team for August 2000 and January 2003. Although being the best available data, MODIS- emissivity measurements suffer from certain error sources, such as snow surface, clouds cover, or over anonymous high water vapor regions. In this work, we also use the corresponding MODIS land cover and leaf area index (LAI) to demonstrate the dependence of emissivity ε on surface types.

CLM is the recently released community land surface model for coupling with NCAR Community Atmospheric Model CAM (Bonan et al. 2002). CLM, a model developed by multiple agencies in a communal effort, is based on previous land surface models, such as BATS (Dickinson et al. 1993), with improved parameterizations for surface snow and hydrology, interception, surface 2m air temperature, and boundary conditions. We used CLM in an offline mode to represent various physical processes among atmospheric-land-ocean applications over the globe. In addition, we performed offline CLM

simulations over Tucson, Arizona, to examine the skin temperature and sensible and latent heat fluxes with the standard bare-soil parameterization of emissivity (0.96) and with average MODIS-observed bare-soil emissivity (~0.90). Further, we used the coupled CAM2/CLM2 to examine emissivity impact in a coupled climate system. Although the absolute values of simulated downward and upward longwave radiation are questionable, partly due to the problematic clouds parameterization in the GCM, the net longwave radiation is much more reliable.

4. Results

4.1. Satellite observed emissivity

Figure 4 compares the geographic distribution of ε in January 2003 and July 2001. In both seasons, Saharan deserts have meaningfully lower ε, with most in ranges 0.88-0.92. In addition, seasonal variations are evident. For example, in the Saharan deserts, ε can be as low as 0.90 in January and to 0.93 in July, with several pixels having extreme low values of 0.75 (Nevertheless, this low values might be retrieval uncertainty, Wan personal communication 2004). This may result from the changes of surface wetness or vegetation conditions. Most rainfall in the Sahara occurs from December through March, so in January the soil is relatively wet compared to June through August. In January, low ε (0.94-0.96) occurs over Eurasia high latitudes, due to the low LAI over forests there.

Australia also shows low ε, about 0.90-0.96 all year. The dependence of ε on LAI vegetation density and species is also evident. For the Boreal forest, the ε ranges from 0.92-0.97 between spring and autumn (not shown).

Due to some retrieval problems for January and July, winter and summer ε data are not always reliable at this point, but better data will be available in the near future. However, the general understanding based on MODIS is that, for vegetated areas, winter has a lower ε than summer due to the growth of vegetation as bare soils have lower ε than vegetation.

Figure 5 shows the ε, skin temperature, and upward longwave radiation along the latitude of New York (~42°N) across North America for July 2001. Emissivity does not depend on the object's temperature but varies with the surface land cover. Closely similar shapes are observed on upward longwave radiation and skin temperature, implying that, over mid-latitude vegetation areas, the skin temperature plays a more significant role in flux and radiation calculation than that of ε. This is easy to understand since according to the Stefan-Boltzmann law, upward longwave radiation depends on skin temperature in a power of 4.

Figure 6 shows ε for different land covers and corresponding histogram. Significant variations, ranging from 0.87 to 0.97 are observed for bare soil (Fig. 6c), with about 17% peak at 0.93 and 12% at 0.95 (Fig. 6d). Such large variations are partly due to the

underlying soil conditions and partly due to the growing state of sparse vegetation. Interestingly, the minimum ε is observed at mid-latitude Northern Hemisphere desert areas (30°N), with values of 0.86. For comparison, the range of ε for mixed forest (Fig. 6e) is much more moderate than that of bare soil, with the maximum ε as 0.98 and lower limit as 0.93. Its histogram has evident peaks at 0.95 and 0.96 above 60% and small percentage at other values. Higher and lower values are observed, but rarely, and are considered as contamination from other surface types. Similar ranges are observed on grasslands (Fig. 6a,b). This agrees with the current understanding that ε varies little over vegetated areas. Fig. 6g-h are for urban areas. Due to the much smaller portion of city numbers over the globe, city has ε ranging from 0.90 to 0.96, regardless of some extreme changes above or below this range. The peak percentage of city is at 0.945-0.955.

Figure 7 shows two samples for snow spectral ε. Snow ε varies with snow surface roughness, snow water content, and snow particle size. An overall value of 0.99 is observed for infrared wavelength, suggesting the broadband ε is close to 0.99.

Canopy ε is more uniform than soil ε. Figure 8 shows the LAI and ε relationship over the mid-eastern USA (27-55°N, 57-115°E), as shown in the map (Fig. 8a). The data is for July, from MODIS observations. In this month, LAI over the selected regions varied from 0 to 6. Emissivity varied from 0.92 to 0.98. The mean ε for each LAI is about 0.96.

Standard deviation in Fig. 8c represents the spread of ε. A noteworthy observation is that, for almost all LAI values, the standard deviations are as low as 0.005-0.01.

The ε of a natural surface is function of vegetation density and structure, which can be partly represented in LAI. Figure 9 shows the variations of LAI for 40°S-40°N, along 20°E longitude. There is a rough relation observed: the lowest LAI corresponds to the lowest. A decrease in LAI from 5°N-16°N corresponds to a decrease in ε from 0.97 to 0.92. The lowest values of ε occur in 15-30°N desert regions, where LAI is not defined--the vegetation barely exists. The correlation coefficient between LAI and ε is 0.67. It appears that that the region from 35°S to about 17°S is barren, yet it seems to have a high emissivity (0.955-0.972), this is because that vegetation there is small in LAI but still has shrub structure. Further, the region from 17°S to 8°S has small LAI values similar to those for 10°N to 16°N, but emissivities are quite different for the two regions. This may be because the structure of vegetation there are different, and LAI is not the best variable to represent vegetation structure.

4.2 Emissivity impacts on land surface modeling

Sensitivity Results from the Offline Land Surface Model

For snow-free grids, CLM2 has bare soil emissivity and canopy emissivity. Since canopy emissivity doesn't vary much, here we focus on examining the impacts of soil emissivity using offline CLM2. The control run uses default ε (0.96 for bare soil, 0.97 for

vegetation. Note in these experiments, we set 0.97 for vegetation-covered regions.) The sensitivity run uses MODIS-observed typically emissivity 0.90[3] for bare soil (namely, 0.90[4]). Figure 10 is the global map of the ground temperature difference between control run and sensitivity run for one day in January. Changes are most significant over desert areas, consistent with our previous theoretical analysis. In general, with soil emissivity set as 0.90, the modeled ground temperature increases about 0.5-1°C with the maxima increase at the Sahara and its nearby regions. Meanwhile, the difference of 2m surface air temperature exhibits changes similar to those noticed over desert areas but with relatively small changes in magnitude, due to the delay of atmosphere response to surface energy input (not shown).

Figure 11 is the difference of SH, sensitivity run minus control run. Again, similar changes are noticed over desert areas with flux increases up to 5Wm^{-2} for Saharan regions, due to the increase of ground temperature. Many other regions over the globe have opposite change, namely a decrease in SH. Figure 12 shows the changes in upward LW. Again, the largest changes are observed over Saharan desert regions, with 1-5Wm^{-2}. Other regions such as Australia, Southwest of USA, south part of Africa, and east Asia around 50°N, 120°E have similar changes. Although the magnitude of SH and LW change are relatively small (<5Wm^{-2}), it is annual mean and instantaneous value can be

[3] We also conducted sensitivity runs by setting soil emissivity as 0.86, 0.92 and 0.94. The patterns of the impact are similar as presented here, with the magnitude differing a little.
[4]

much higher. Therefore, we need to examine the diurnal variations and seasonality of this error. More importantly, we need to examine the error in a real surface-atmosphere climate system using a coupled GCM.

Since the largest impacts of ε are over desert areas, we conducted further model sensitivity studies over one of these areas: Tucson, Arizona, USA (~30°N, 112°W). The atmospheric input is based on observations. The control run uses the default emissivity of CLM (0.96), and the sensitivity run keeps everything the same as the control run except for setting soil emissivity as 0.90, which is the observed typical value for soil there. The runs start at Julian day 132, 1993, with output every 20 minutes and averaged to daily mean (as presented here).The comparison shows that skin temperature with ε = 0.90 is lower than that of ε = 0.96, with the difference in general as -4°C (Fig. 12 a). During some daytime periods, the difference can be as high as 10K (can see from 20-minute output). At nighttime, the difference is little. Similarly, sensible and latent heat flux changes between control and sensitivity runs are also very large, 10 Wm^{-2} to as high as 50Wm^{-2} (Figure 12 b and c). Furthermore, the changes of latent heat flux can be negative. It seems that the impact of ε on sensible heat flux is larger than it is on latent heat flux since the soil moisture is very low.

The Tucson study (Figure 13) is more reliable as the atmosphere forcing data in this case are the real observations, and thus the magnitude and sign were reliable. By contrast, in the offline CLM sensitivity study (Fig. 10), the atmosphere forcing was from the NCEP

reanalysis, which has reported problem in their surface wind and surface air temperature (Trenberth 2002, personal communicaition). Another evidence is that Figure 13 from the coupled CAM2/CLM2 also shows that current high-constant emissivity induces warm bias at surface, which is consistent with Figure 13 but not with Figure 10. Nevertheless, we still need to keep offline CLM study here to show that the land model by itself is sensitive to the emissivity.

Results from Coupled GCM

In a coupled climate system, the uncertainties and impacts of ε may propagate into the atmosphere and the atmosphere noise may enhance or reduce ε impact on surface. Therefore, it is interesting to study the ε effects in the land-atmosphere climate system using GCM. We conduct a series of sensitivity runs using NCAR CAM2/CLM2. To avoid spin-up, we use NCAR specifically recommended initial condition and boundary condition files for the land surface model. Similar to offline runs, the control run set ε as default values, and the sensitivity run sets the soil ε at 0.90, and canopy emissivity at 0.97. Both control and sensitivity cases run the model for a short time. Running the model for a short time is based on two considerations: first, since in the two runs only ε is changed and any other condition is the same, the differences between the two runs are caused by the ε impacts; second, we noticed that after a long running time, the model output became quite noisy. This may be due to the atmosphere model's noise being transported into model outputs (Dickinson, personal communication, 2003).

Figures 14a and b show the global distribution of surface air temperature. The model gives reasonable simulation for this variable. Figures 14c and d show the ε impacts evident over desert and semi-desert regions. A decrease of ε causes a decrease of surface air temperature. Namely, current high-constant ε results in warm bias over desert regions on surface air temperature field, which can be as high as 1.5°C over Saharan regions. By comparson, emissivity (ε) impact on skin temperature seems to be smaller than its impact on surface air temperature. Figure 15 shows skin temperature decreases as much as 1-1.5°C over certain desert regions of the southwest USA, Eurasia, Australia, and Sahara. The warming bias at surface skin and air levels imply an enhanced sensible heat flux from surface to air. Nevertheless, we notice that over certain small regions, the ε impacts are opposite to the rest of the land regions, such as 0°N, 20°E, where the control case has lower air temperature than the sensitivity case, resulting in a negative value in Fig. 15a. Nevertheless, such negative values are less significant on Fig. 14b, implying that ε impacts on this region is relatively weak, so that the signs of the impact do not always remain evident.

5. Uncertainties and Discussions

Broadband emissivities have uncertainties stemmed from MODIS spectral emissivity ε_λ as well as the conversion equation used to calculate broadband ε from ε_λ. As previously reported, over certain areas of South America and tropical Africa, cloud cover results in

missing ε. It is also questionable over certain Saharan areas, where evident ε changes (3-5%) from January to July occur. Whether such large changes are due to the seasonality of soil wetness or due to retrieval problems is unknown. Nevertheless, in general, MODIS ε shows encouraging accuracy in terms of geographic distribution and inter-annual variations (Wan, personal communication, 2003). In addition, the regression equations used to convert MODIS ε_λ into broadband ε give a statistical average for ε. However, our research shows that uncertainty induced by the regression approach is less than 1%.

From a land surface modeling perspective, the importance of ε has been ignored so far. Compared with surface albedo, which determines the net surface solar radiation, ε may be less critical in the surface energy budget. But it is very important over arid and semi-arid areas and at least should be taken into account there. By changing net longwave radiation from that which was supposed to be from blackbody, ε affects skin temperature, sensible, and latent heat flux simulations. MODIS global ε observations show great value for use in land surface models.

Optimally, use of MODIS observations, or other remotely sensed ε information such as those from the ASTER in land surface models is a continuing task. Two approaches are practical: one is to use a look-up table to show ε variations as a function of latitude, season, and land cover, and then to parameterize ε in the model; another is to directly use MODIS ε observations into the model to replace current prescribed, unrealistic values.

Unfortunately, scaling up ε observations from MODIS fine resolution into the model grid cell requires more research. Because it is difficult to accurately measure ε, and because ε over some biologically distinct cover types are nearly the same, it may be adequate to use single values for each discrete land-cover type to represent ε in a GCM rather than directly input satellite global or regional observations into a model.

Inconsistencies exist in placing satellite-based ε into a land surface model. One is that satellites can only measure spectral band ε_λ; therefore, satellite data need to be converted into broadband. We recommend a regression equation approach in this paper. Another inconsistency is that over partially vegetation-covered regions, the satellite-measured ε, even at a resolution as fine as 1km, is a combination of soil and vegetation emissivities. How to interpret this combined information into a model's canopy and ground ε is a question that needs to be addressed.

The ε impacts presented here are from one model. It is valuable to re-evaluate these impacts using other models and to examine to what extent these impacts are valid. Before a model can be used to examine ε impacts, however, the formulations of land surface need to be carefully checked, since some models derive the land formulations by setting ε as a unit for simplification and ignore certain terms as discussed in Deardoff (1976). Such neglect will cause the ε to have a misleading effect.

Acknowledgements: This work is supported by NASA EOSIDS (PI-R. E. Dickinson) under contract NRA-99-ESA. Thanks go to Dr. G. Bonan of NCAR who provided us NCAR computer account to conduct the coupled model experiments. We especially thank the NOAA CDC reanalysis group for their extremely user-friendly web page where we obtained reanalysis data and analyses (www.cdd.noaa.gov/cdc/reanalysis). Special thanks go to Dr. Z. Wan for providing us MODIS LST/emissivity data and for insightful discussions. And to Dr. P. Thornton, also, who carefully edited the early version of manuscript and provided helpful suggestions.

References

Bonan, G. B., K. W. Oleson, M. Vertenstein, S. Levis, X. Zeng, Y. Dai, R. E. Dickinson, and Z. Yang. 2002. The land surface climatology of the community land model coupled to the NCAR community climate model. *J. of Climate* **15,** 3123-3149.

Deardorff, J. W. Efficient prediction of ground surface temperature and moisture with inclusion of a layer of vegetation. *J. of Geophysical Research* **83(C4),** 1889-1903.

Dickinson, R. E., A. Henderson-Sellers, P. J. Kennedy, and M. F. Wilson. 1986. Biosphere-atmosphere transfer scheme (BATS) for the NCAR community climate model. NCAR Tech. Note/TN-275+STR} . Natl. Cent. for Atmos. Res., Boulder, Colo.

Dickinson, R. E., A. Henderson-Sellers, and P. J. Kennedy. 1993: Biosphere-Atmosphere Transfer Scheme (BATS) Version 1E as Coupled to the NCAR Community Climate Model. NCAR Tech. Note, NCAR/TN-387+STR. National Center for Atmos. Res., Boulder, CO.

Jin, M., R.E. Dickinson, and A. M. Vogelmann. 1997. A comparison of CCM2/BATS skin temperature and surface-air temperature with satellite and surface observations. *J. of Climate, **10**, 1505-1524*.

Francois, C., C. Ottle, and L. Prevot. 1997. Analytical parameterization of canopy directional emissivity and directional radiance in the thermal infrared. Application on the retrieval of soil and foliage temperatures using two directional measurements. *Int. J. Remote Sensing* **18**, 2587-2621.

Idso, S. B., Jackson, R. D., Ehrler, W. L. and Mitchell, S. T. 1969. A method for determination of infrared emittance of leaves. *Ecology* **50**, 899-902.

Liang, S. 2001. An optimization algorithm for separating land surface temperature and emissivity from multispectral thermal infrared imagery. *IEEE Transactions on Geosciences and Remote Sensing,* **39**, 264-274.

Liang, S. 2003. *Quantitative Remote Sensing of Land Surfaces***, CITY:**John Wiley and Sons..

Logan, L. M., G. R. Hunt, and J. W. Salisbury. 1974. The use of mid-infrared spectroscopy in remote sensing of space targets. In *Infrared and Raman Spectroscopy of Lunar and Terrestrial Materials,* edited by C. Karr. San Diego: Academic.

Nerry, F., J. Labed, and M. P. Stoll. 1990. Spectral properties of land surfaces in the thermal infrared 1. Laboratory measurements of absolute spectral emissivity signatures. *J. of Geophysical Res.* **95**, 7027-7044.

Prabhakara, C. and G. Dalu. 1976. Remote sensing of the surface emissivity at 9μm over the globe. *J. of Geophysical Research*, **81**, 3719-3724.

Rowntree, P. R. 1991: Atmospheric parameterization schemes for evaporation over land: Basic concepts and climate modeling aspects. In *Land surface evaporation measurement and parameterization,* edited by T. J. Schmugge and J. Andre. CITY: Spring-Verlag.

Sellers, PJ, Y. Mintz, YC Sud, A. Dalcher. 1986. A simple biosphere model (SiB) for use within general circulation models. *J. of Climate* **9**, 738-763.

Snyder, W. C., Z. Wan, Y. Zhang, and Y.-Z. Feng. 1998. Classification-based emissivity for land surface temperature measurement from space. *Int. J. Remote Sensing* **19**, 2753-2774.

Van De Griend, A. A. Van, and M. Owe 1993. On the relationship between thermal emissivity and the normalized difference vegetation index for nature surfaces. *Int. J. Remote Sensing* **14**, 1119-1131.

Wan, Z. and Z. Li 1997 A physics-based algorithm for retrieving land-surface emissivity and temperature from EOS/MODIS data. *IEEE Trans. Geosci. Remote Sens.* **35**, 980-996.

Zhou, L, R. E. Dickinson, T. Yu, M. Jin et. al., 2003: A sensitivity study of climate and energy balance simulations with use of satellite derived emissivity data over Northern Africa and the Arabian Peninsula. *J. Geophys. Res.*, **108**(D24), 4795, doi:so.1029/2003JD004083.

Figure Captions

Figure 1 (a). NCEP/NCAR reanalysis for July 2001, surface net longwave radiation. (b) Same as Fig.1a, but for November 2001. (c) Same as Fig.1a, but for annual mean for year 2001.

Figure 2: Lab measured soil emissivity. Data were obtained in June 2002, from Z. Wan's webpage with permission, http://www.icess.ucsb.edu/modis/EMIS/html/em.html.

Figure 3: (a). MODIS broadband emissivity for January 2003. The broadband emissivities are derived from the MODIS spectral band emissivities using regression-equation-based MODTRAN simulation. The resolution of original MODIS emissivity data is 1km and here is averaged to T42 resolution. (b) Same as Fig. 3a, but for July 2001.

Figure 4: Examination of 3-band calculated broadband emissivity versus 7 MODIS band calculated broadband emissivity.

Figure 5: Emissivity, upward longwave radiation, and skin temperature for latitude 42°N. Data is from MDOIS observation. Spatial data resolution is 5km.

Figure 6: (a). All grassland pixels over the globe from MODIS. The emissivity values in the V4 MODIS Land-Surface Temperature/Emissivity product (MOD11B1) at 5km sinusoidal grids. The x-direction is latitude but in ISIN projection (i.e., 0 is 90N, the 4380 is 90S, 2190 is equator). (b) is the corresponding histogram in percentage for Grassland based on the data in (a). (c) is for barren and sparsely vegetated areas, namely MODIS land cover type16. (d) is the histogram based on

(c). (e) is for mixed forest (MODIS land cover type 5); and (f) is the histogram based on (e). (g) is for urban areas; and (h) is the histogram based on (g).

Figure 7: Samples of snow spectral emissivity. Data is copied from Wan's emissivity lab with permission in 2002.

Figure 8: The relationship between LAI and emissivity. (a) The map shows the study regions, and (b) is the LAI vs. emissivity; (c) is the standard deviation of emissivity for each LAI value.

Figure 9: LAI and emissivity relationship for 40°N-40°S, and 20°E. The open circle is LAI and dotted line is for emissivity. The scale of emissivity is (emissivity *10).

Figure 10: Offline CLM simulated difference between control run (ε = 0.96 as default) and sensitivity run of soil emissivity as 0.90, for ground temperature. The data is for daily averages of January 1998. Unit is Kelvin.

Figure 11: Same as Fig. 9 except for sensible heat flux. Unit is Wm^{-2}.

Figure 12: Same as Fig. 9 but for net longwave radiation. Unit is Wm^{-2}.

Figure 13: Offline CLM simulations for Tucson, 1993. Presented are difference between the run with emissivity settled as the observed value (0.90) and the run with the default emissivity (0.96). a) is for skin temperature, (b) for sensible heat flux, and (c) for latent heat flux from surface to air.

Figure 14: Emissivity impacts in the coupled model CAM2/CLM2: (a) control run of one day daily averaged surface air temperature; (b) control run of another daily averaged surface air temperature; (c) emissivity impact on surface air temperature, control run minus sensitivity run; (d) the same as (c) but for another day.

Figure 15: Coupled CAM2/CLM2 simulated emissivity impact on surface temperature fro two random days of September. The difference is control run minus sensitivity run. The control run uses CLM default soil emissivity (ε=0.96), and sensitivity run uses satellite observed emissivity at T42 resolution. Unit is Kelvin.

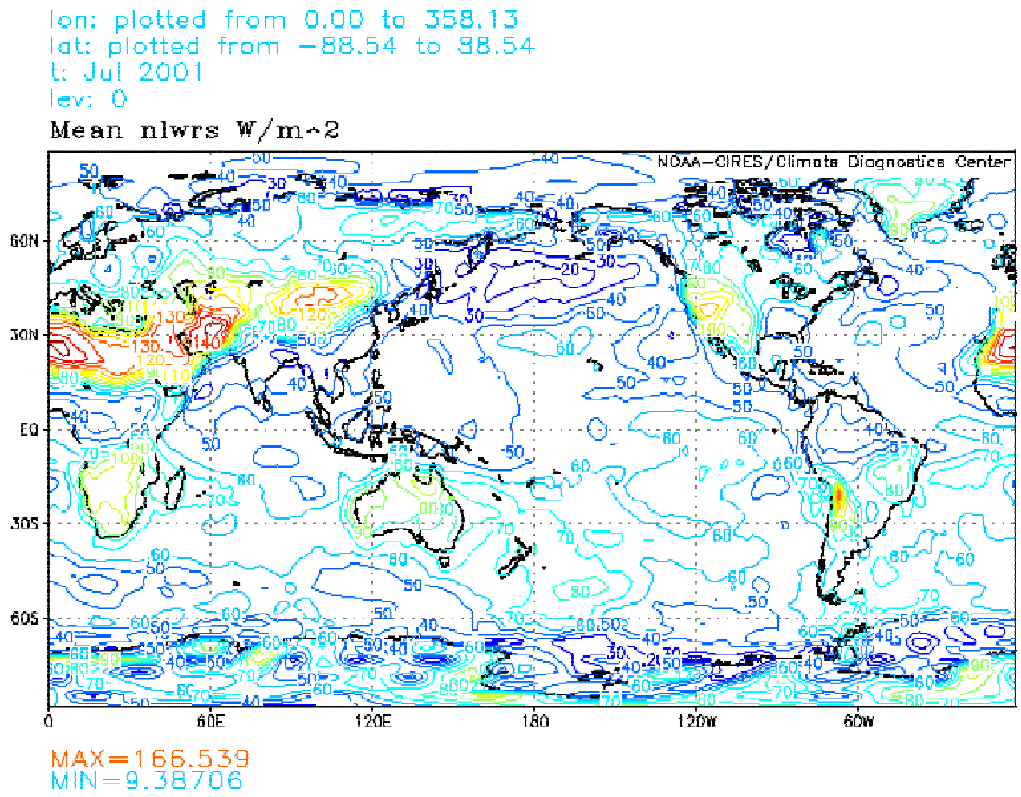

Fig. 1a. NCEP/NCAR reanalysis for July 2001, surface net longwave radiation.

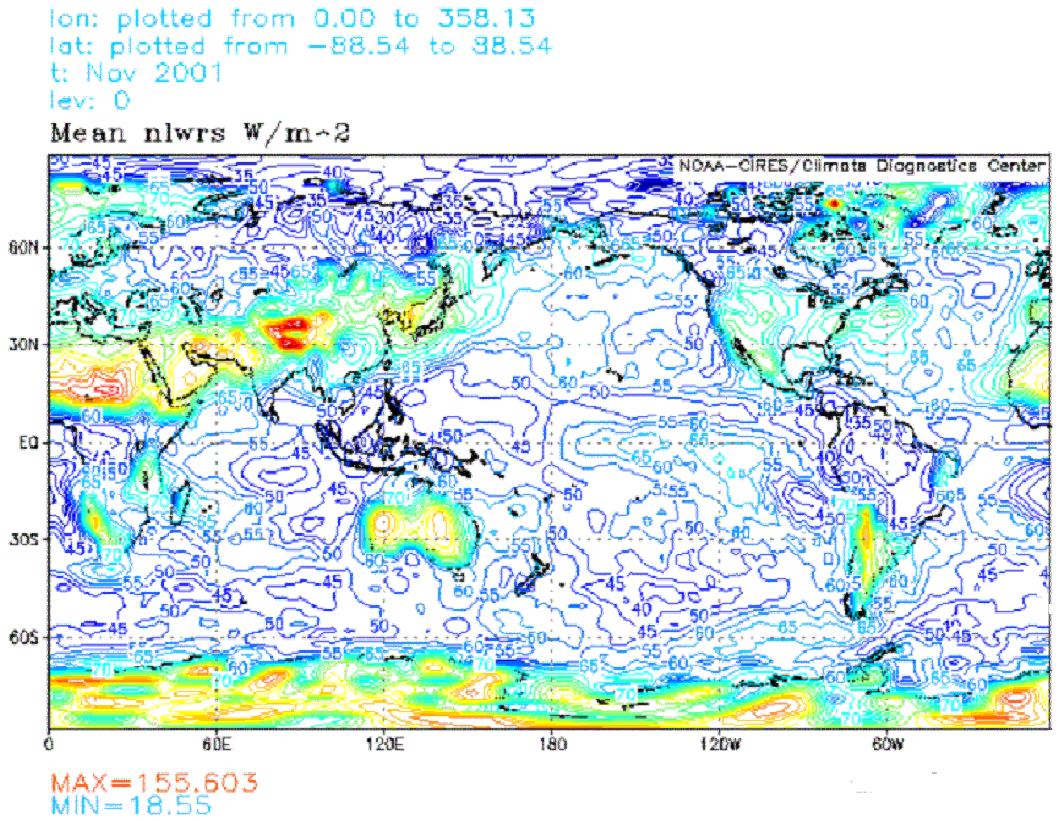

Fig. 1b Same as Fig.1a, but for November 2001.

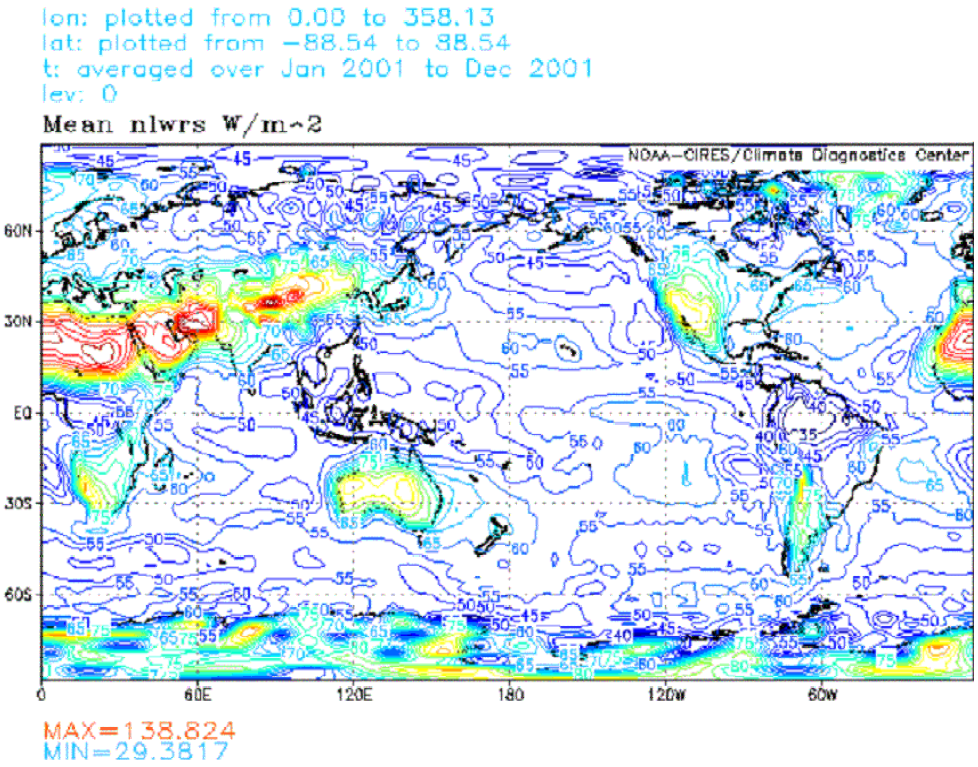

Fig.1c Same as Fig.1a, but for annual mean for year 2001.

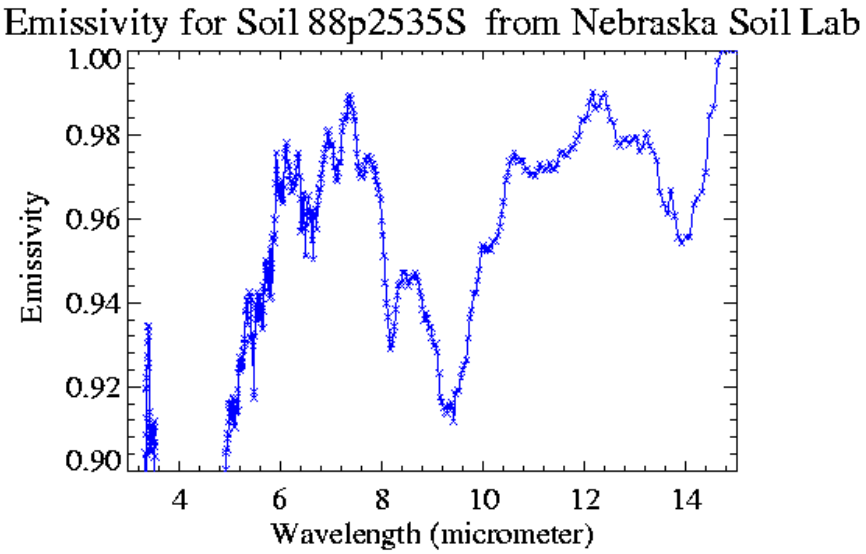

Figure 2: Lab measured soil emissivity. Data were obtained from Z. Wan's webpage in 2002 with permission, http://www.icess.ucsb.edu/modis/EMIS/html/em.html.

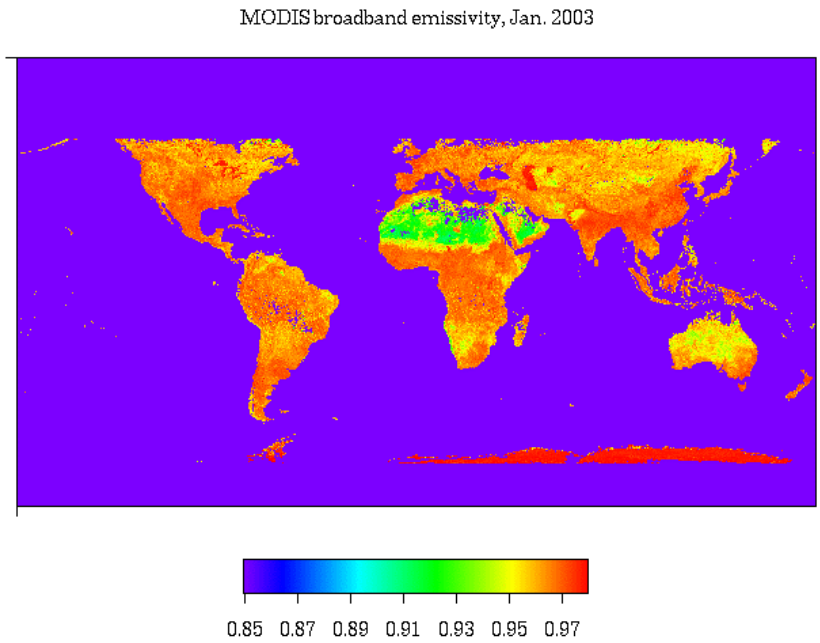

Fig3a. MODIS broadband emissivity for January 2003. The broadband emissivities are derived from the MODIS spectral band emissivities using regression-equation-based MODTRAN simulation. The resolution of original MODIS emissivity data is 1km and here is averaged to T42 resolution.

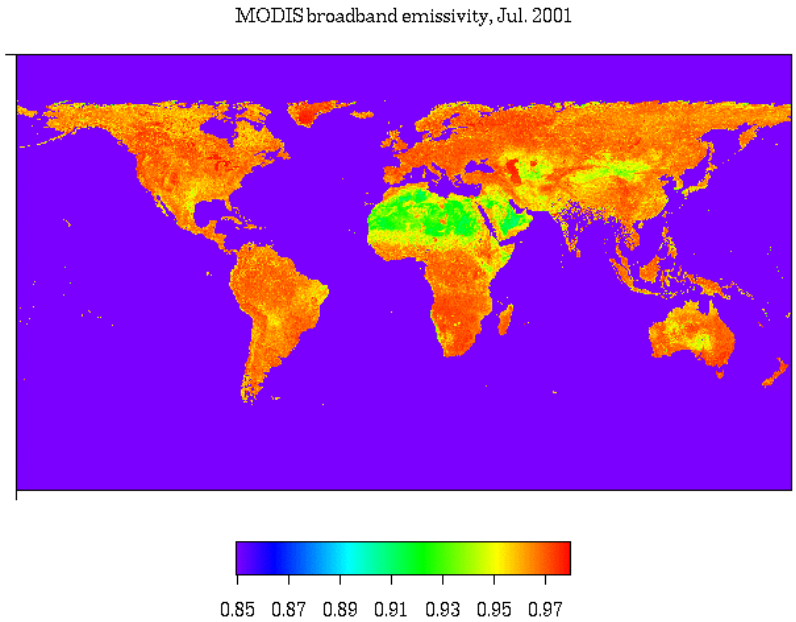

Fig. 3b Same as Fig. 3a, but for July 2001.

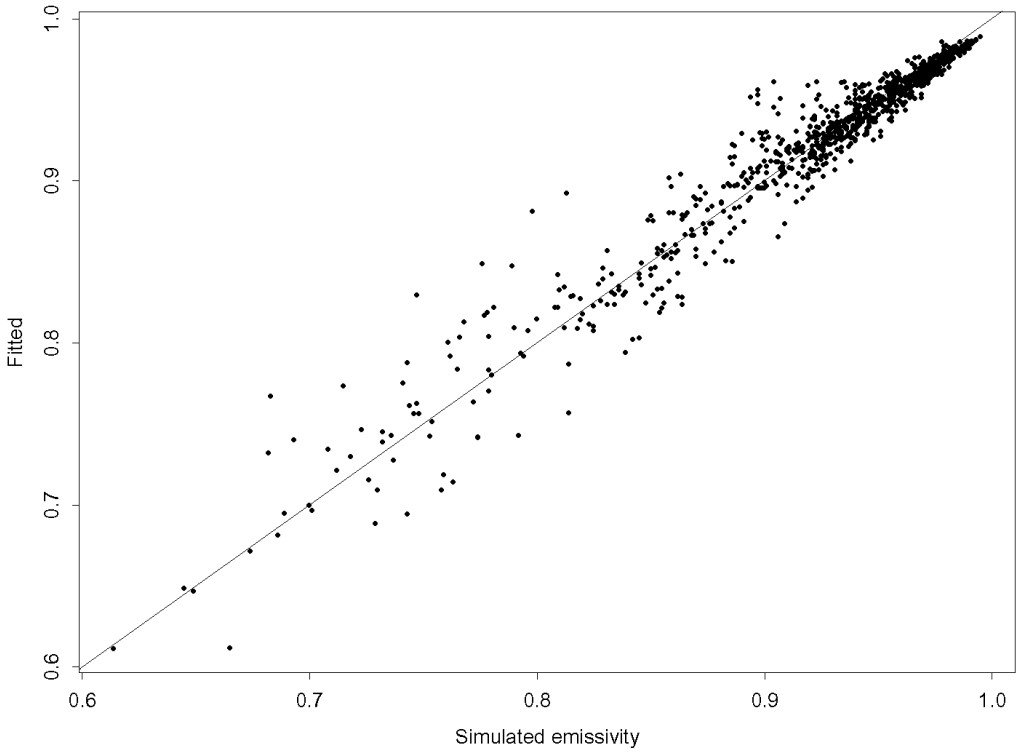

Figure 4: Examination of 3-band calculated broadband emissivity versus 7 MODIS band calculated broadband emissivity.

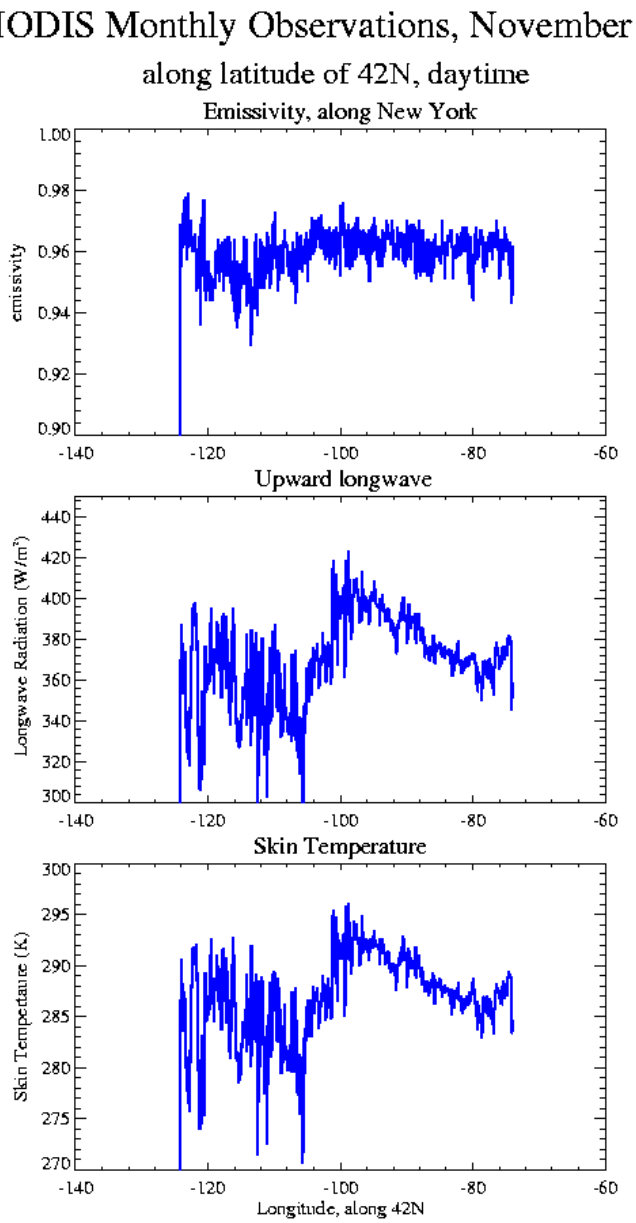

Figure 5: Emissivity, upward longwave radiation, and skin temperature for latitude 42°N. Data is from MDOIS observation. Spatial data resolution is 5km.

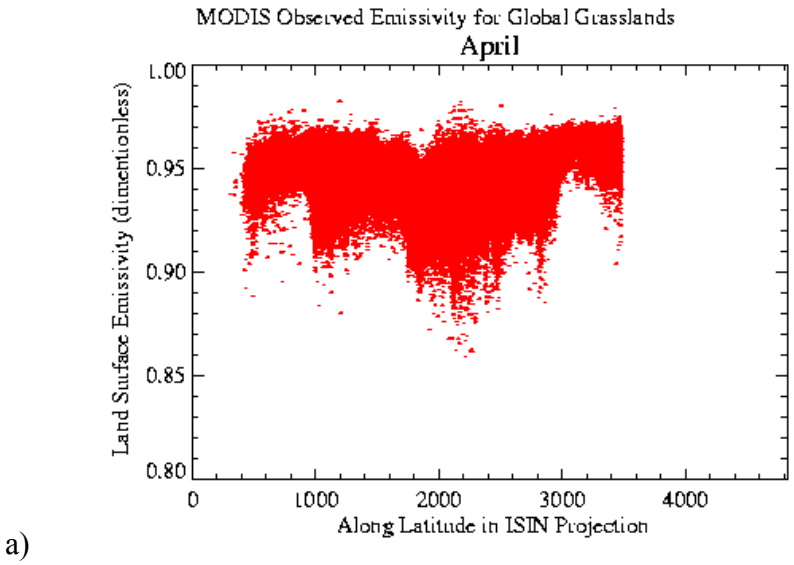

a)

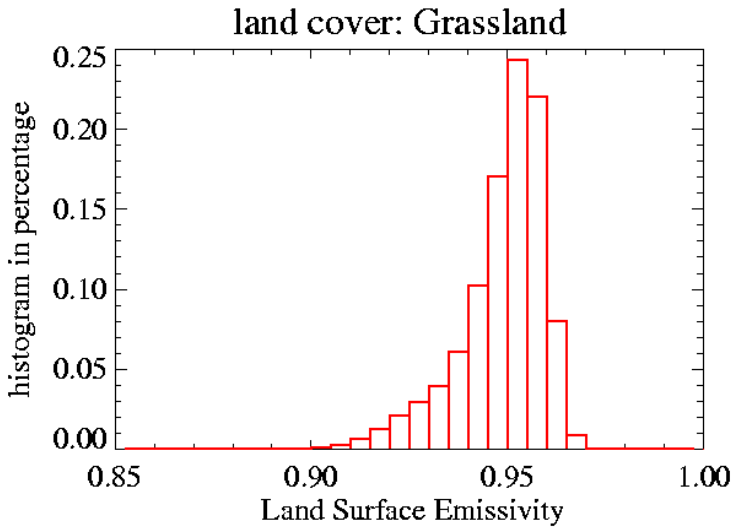

b)

Figure 6a. All grassland pixels over the globe from MODIS. The emissivity values in the V4 MODIS Land-Surface Temperature/Emissivity product (MOD11B1) at 5km sinusoidal grids. The x-direction is latitude but in ISIN projection (i.e., 0 is 90ºN, the 4380 is 90ºS, 2190 is equator). (b) is the corresponding histogram in percentage for Grassland based on the data in (a).

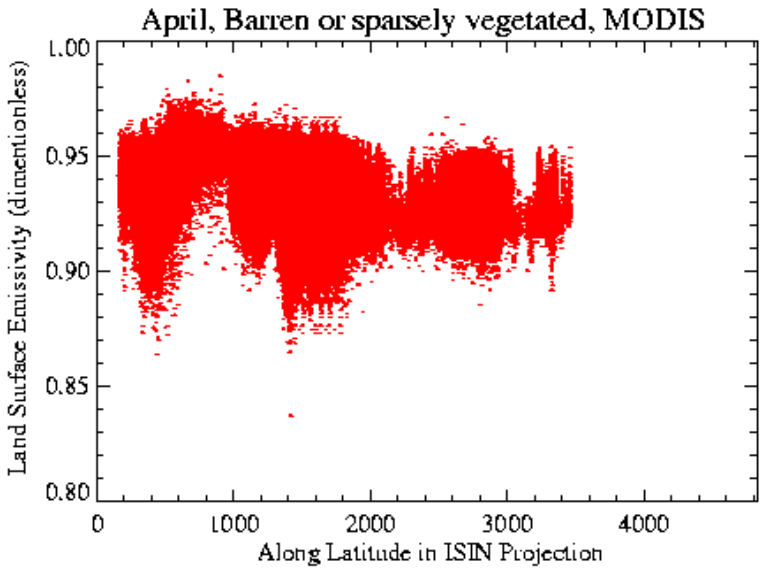

(c)

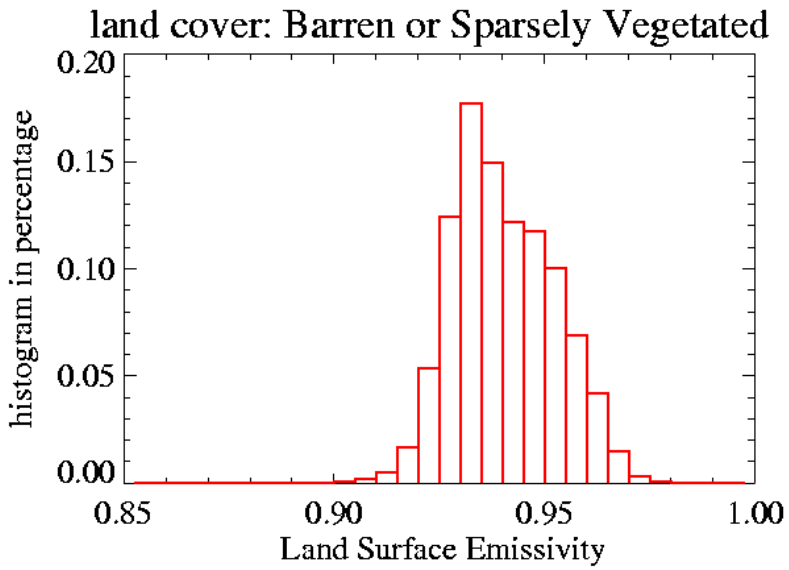

(d)

Fig. 6c: For barren and sparsely vegetated areas, namely MODIS land cover type16. (d) is the histogram based on (c).

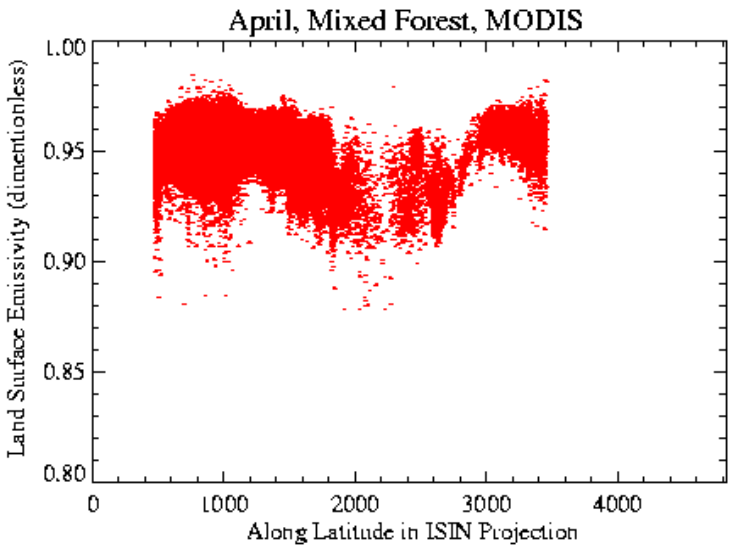

(e)

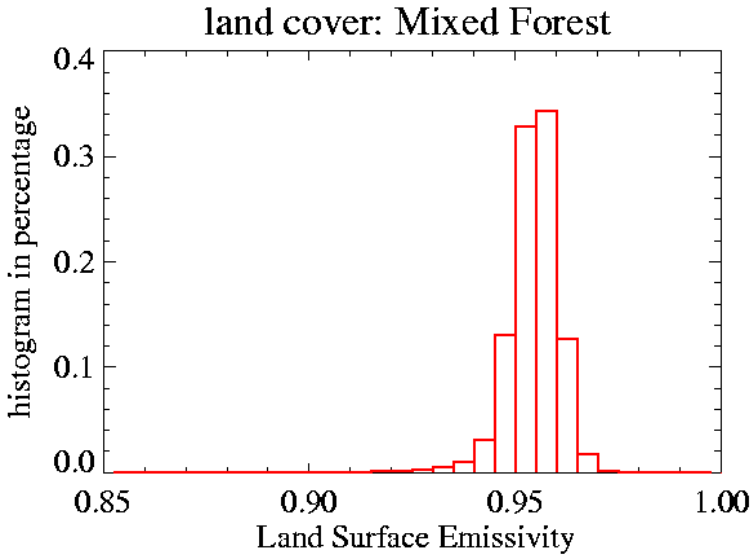

(f)

Fig. 6e. For mixed forest (MODIS land cover type 5); and (f) is the histogram based on e.

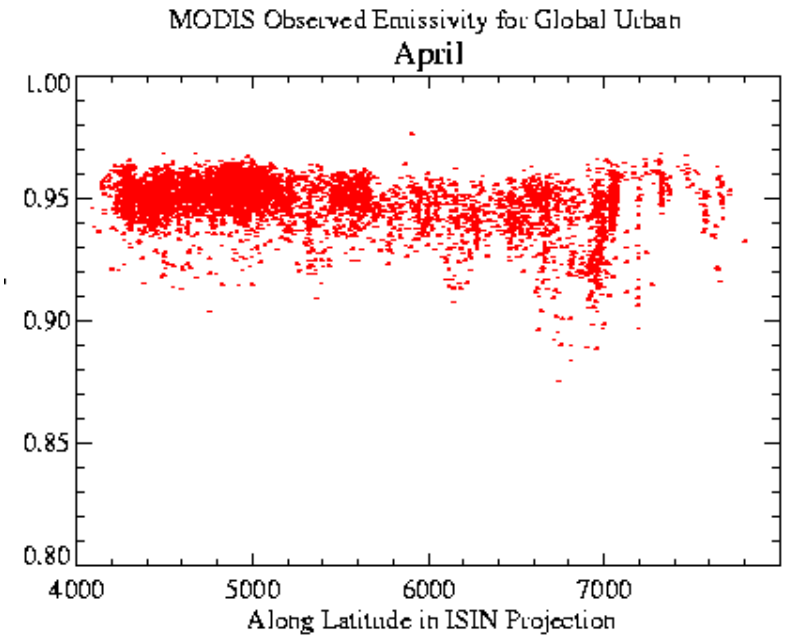

(g)

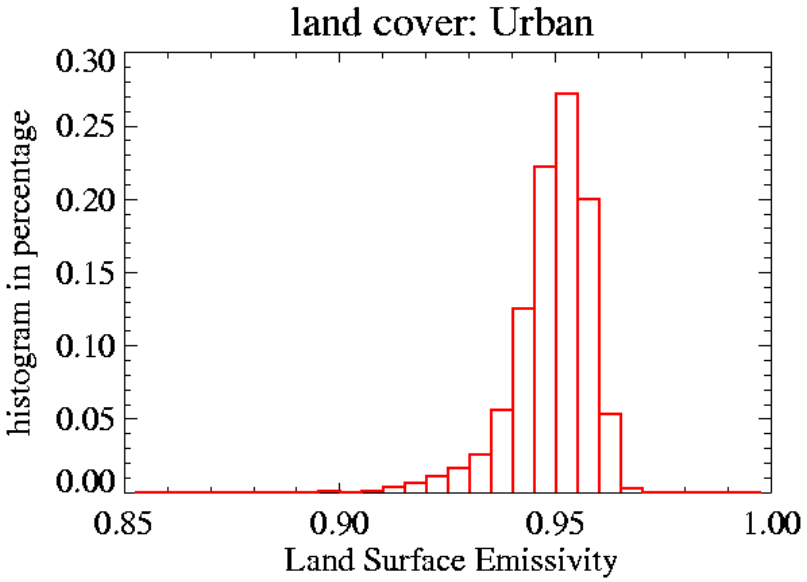

(h)

Fig.6g: Urban areas; and (h) is the histogram based on (g).

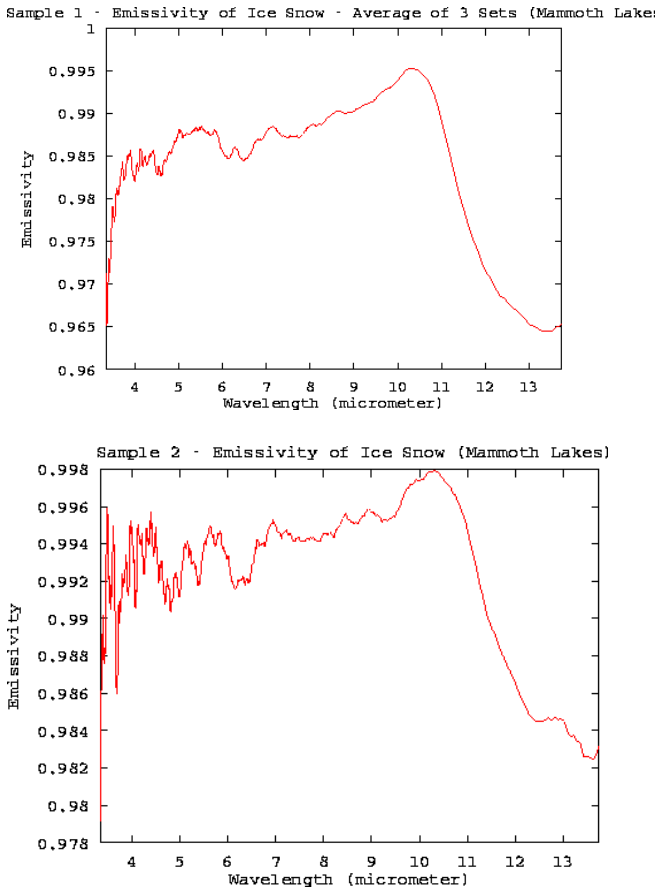

Figure 7: Samples of snow spectral emissivity. Data is copied from Wan's emissivity lab in 2002 with permission.

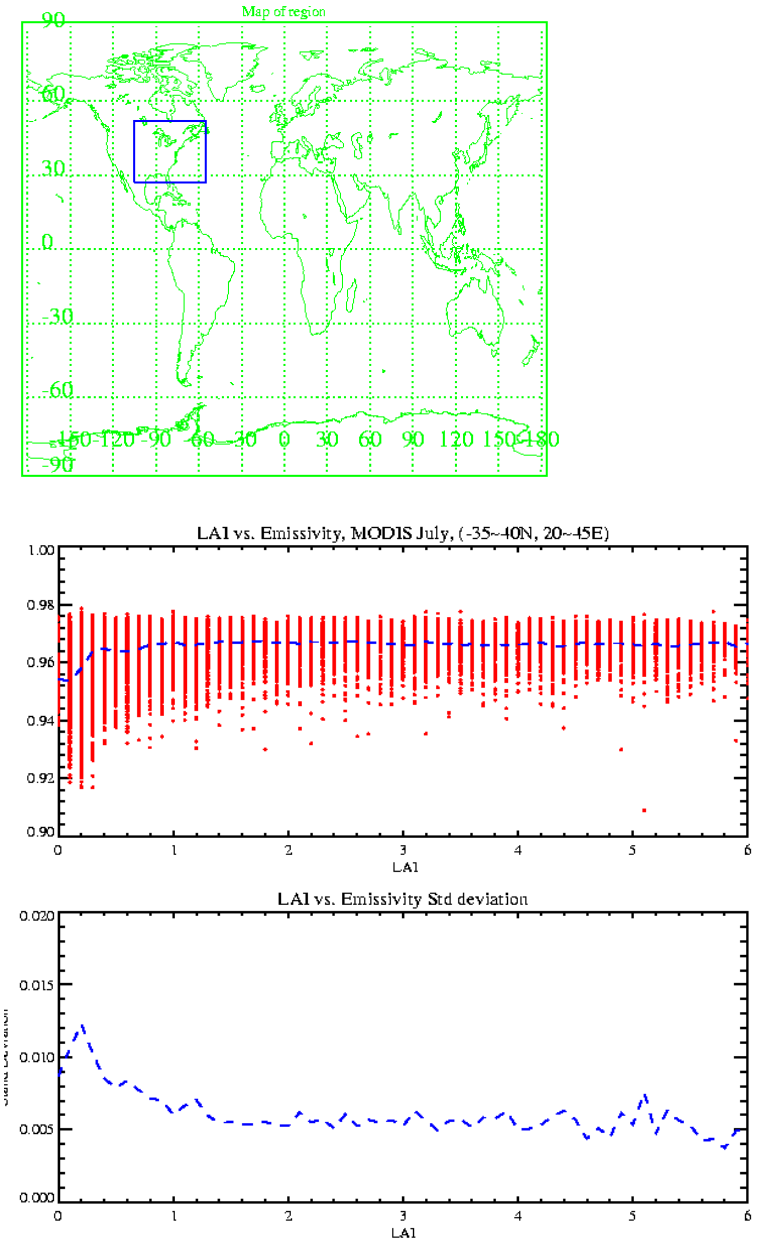

Figure 8: The relationship between LAI and emissivity. (a) The map shows the study regions, and (b) is the LAI vs. emissivity; (c) is the standard deviation of emissivity for each LAI value.

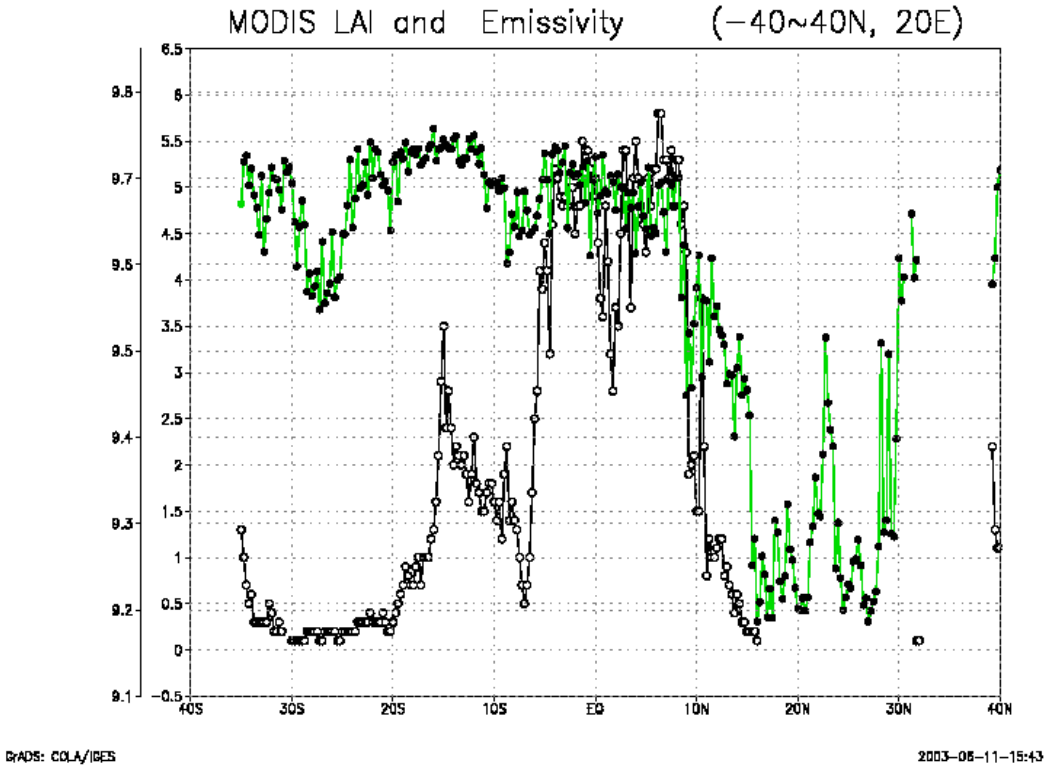

Figure 9: LAI and emissivity relationship for 40°N-40°S, and 20°E. The open circle is LAI and dotted line is for emissivity. The scale of emissivity is (emissivity *10).

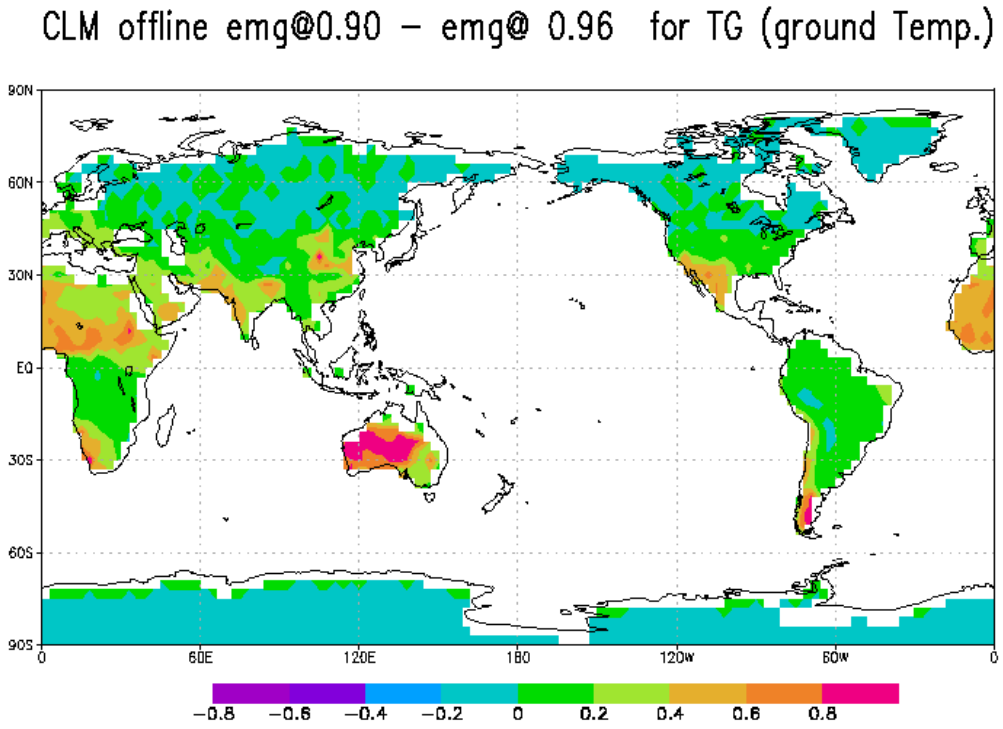

Figure 10: Offline CLM simulated difference between control run (ε = 0.96 as default) and sensitivity run of soil emissivity as 0.90, for ground temperature. The data is for daily averages of January 1998. Unit is Kelvin.

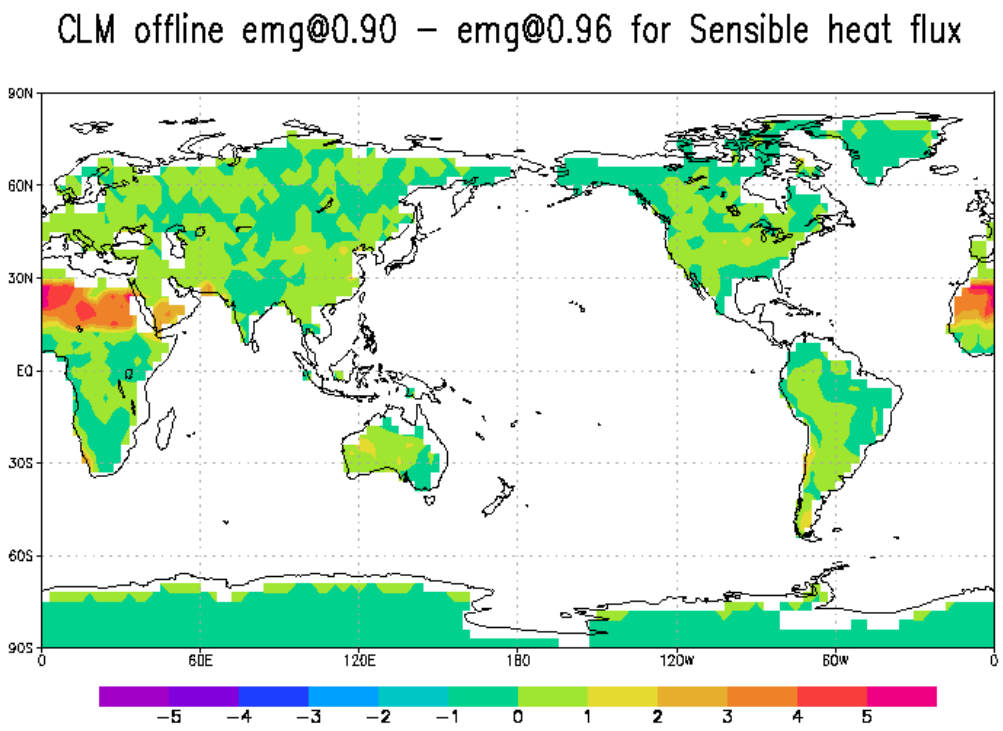

Figure 11: Same as Fig. 9 except for sensible heat flux. Unit is Wm^{-2}.

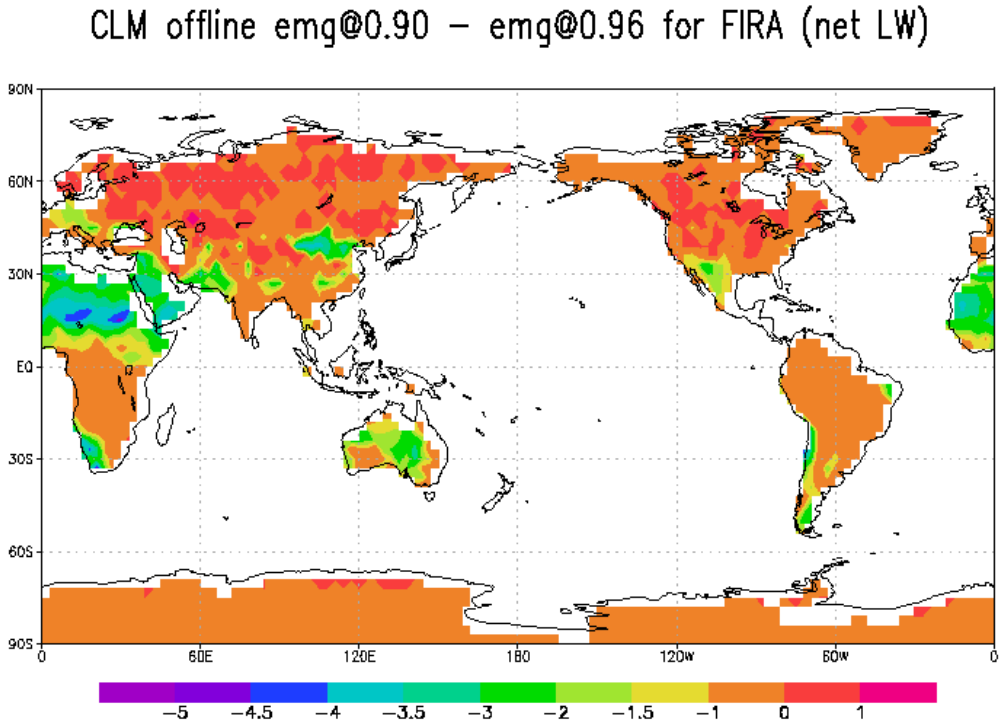

Figure 12: Same as Fig. 9 but for net longwave radiation. Unit is Wm^{-2}.

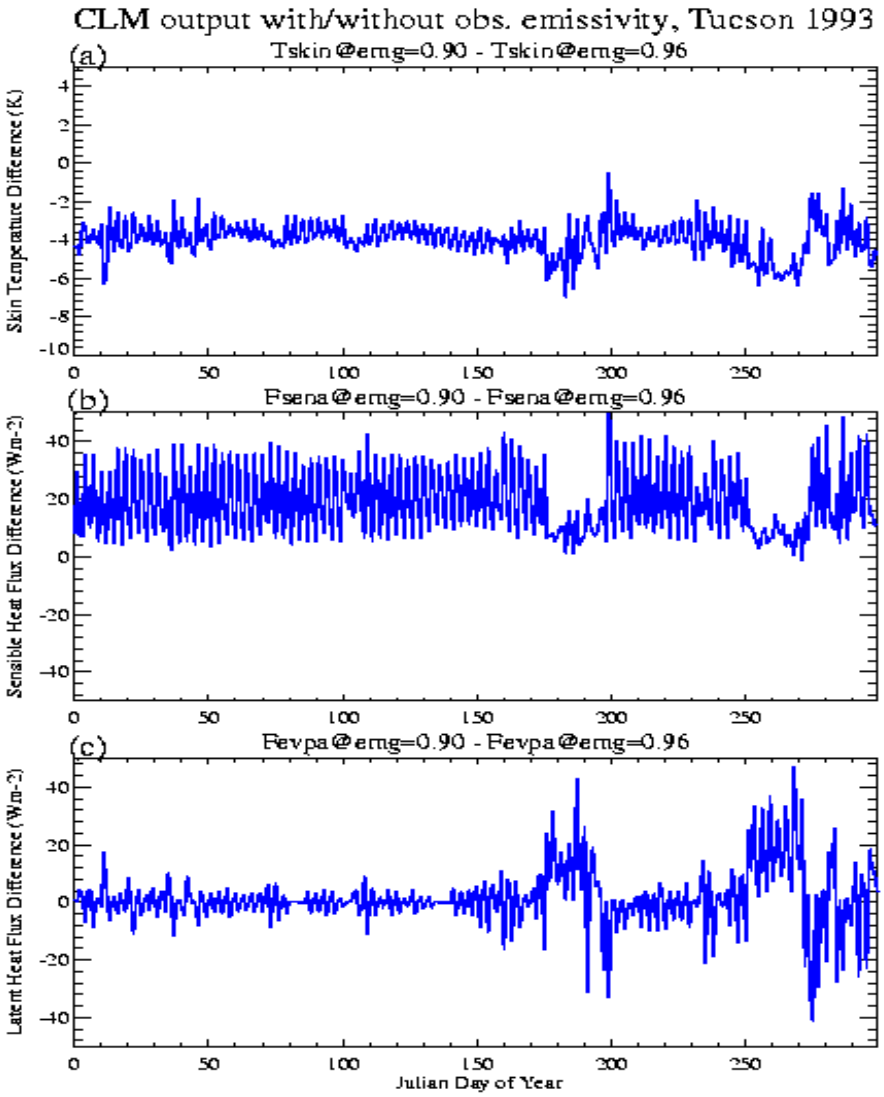

Figure 13: Offline CLM simulations for Tucson, 1993. Presented are difference between the run with emissivity settled as the observed value (0.90) and the run with the default emissivity (0.96). a) is for skin temperature, (b) for sensible heat flux, and (c) for latent heat flux from surface to air.

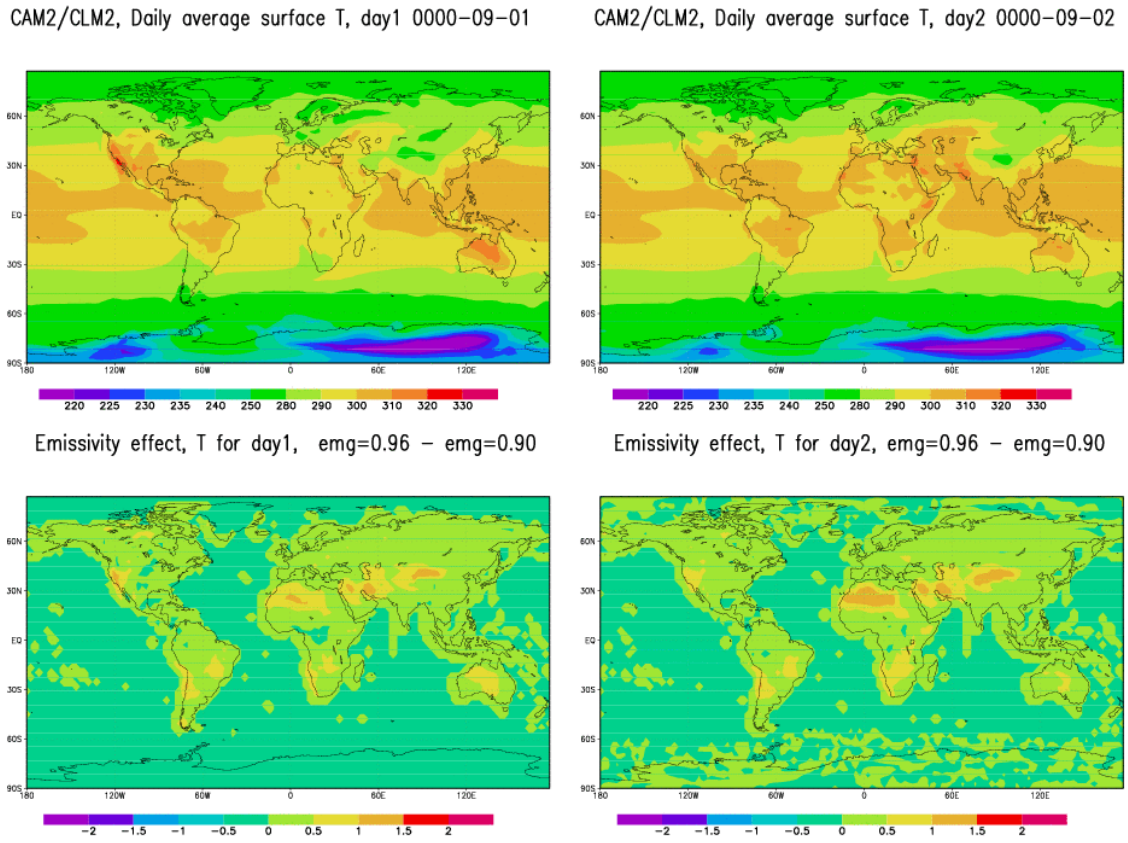

(a)(b)
c)(d)
Figure 14: Emissivity impacts in the coupled model CAM2/CLM2: (a) control run of one day daily averaged surface air temperature; (b) control run of another daily averaged surface air temperature; (c) emissivity impact on surface air temperature, control run minus sensitivity run; (d) the same as (c) but for another day.

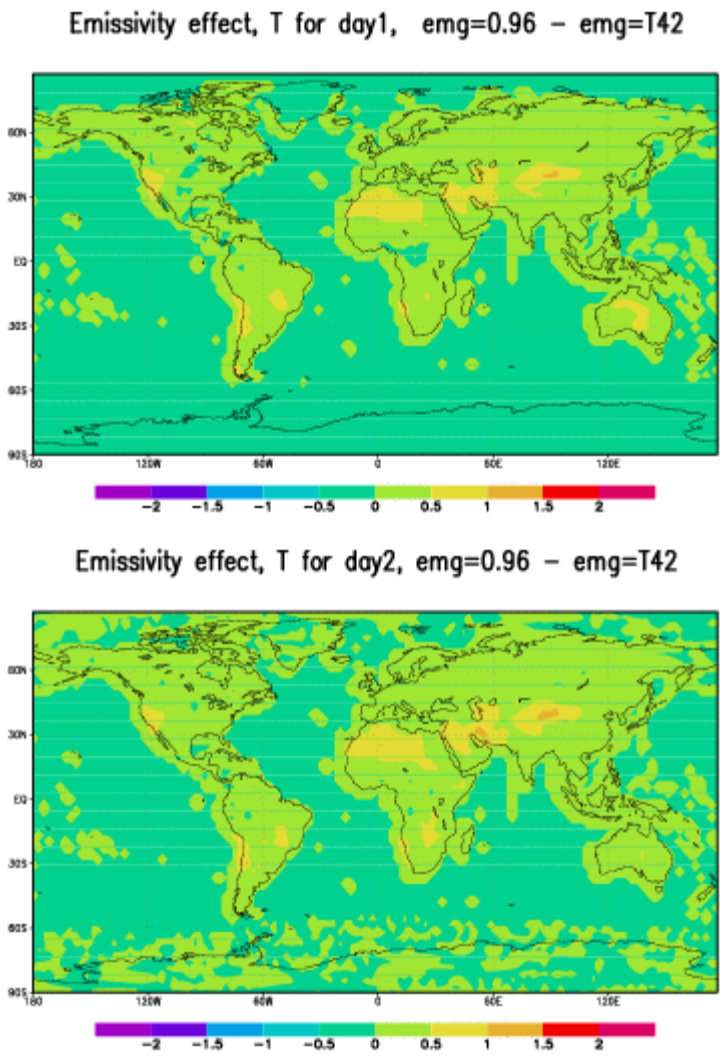

Figure 15: Coupled CAM2/CLM2 simulated emissivity impact on surface temperature fro two random days of September. The difference is control run minus sensitivity run. The control run uses CLM default soil emissivity (ε=0.96), and sensitivity run uses satellite observed emissivity at T42 resolution. Unit is Kelvin.

Table 1: Emissivity table of some common materials. This is not a comprehensive list and should be taken as a reference only. (Copied from http://www.electro-optical.com/)

Material	**ε**
Aluminum foil	0.04
Asbestos board	0.96
Asbestos paper	0.93
Asphalt (paving)	0.97
Brass (hard rolled - polished w/lines)	0.04
(some what attacked)	0.04
Brick (red - rough)	0.93
Brick (silica - unglazed rough)	0.80
Carbon (T - carbon 0.9% ash)	0.81
Concrete	0.94
Copper (plate heavily oxidized)	0.78
Frozen soil	0.93
Glass (smooth)	0.94
Gold (pure highly polished)	0.02
Granite (polished)	0.85
Ice	0.97
Marble (light gray polished)	0.93
Paper (black tar)	0.93
Paper (white)	0.95
Plaster (white)	0.91
Plywood	0.96
Tin (bright tinned iron sheet)	0.04
Water	0.95
Wood (freshly planned)	0.90